Topics in Catalysis
https://doi.org/10.1007/s11244-025-02177-x

ORIGINAL PAPER

NiFe Catalysts Supported on Nb_2O_5 for Enhanced Hydrodeoxygenation: A Study on Performance and Selectivity

Telis Naiara[1,2] · Campos Fraga Mariana[1] · Zevaco Thomas[1] · Raffelt Klaus[1] · Soares Ricardo[2]

Accepted: 5 August 2025

Abstract
Biomass-derived bio-oils, particularly those obtained from fast pyrolysis, offer a renewable alternative to fossil fuels. However, their high oxygen content and low stability limit their direct use as transportation fuels. Catalytic hydrodeoxygenation (HDO) represents a promising strategy to increase the quality of bio-oil by removing oxygen from organic compounds. This study investigated the catalytic performance of monometallic and bimetallic Ni–Fe catalysts supported on Nb_2O_5 and SiO_2 for the hydrodeoxygenation (HDO) of guaiacol, a model compound representative of bio-oil derived from lignin. The catalysts were synthesized, characterized, and tested under identical conditions to evaluate the effects of metal composition, support properties, and reaction temperature on activity and selectivity. Compared with their monometallic counterparts, bimetallic Ni–Fe catalysts demonstrated superior performance, with the $5Ni1Fe/Nb_2O_5$ catalyst achieving the highest guaiacol conversion (59%) and enhanced selectivity toward cyclohexanol (34%) and cyclohexane (10%) at 300 °C. The synergistic interaction between Ni and Fe facilitated hydrogenation and hydrogenolysis pathways, whereas the acidic and oxophilic properties of Nb_2O_5 promoted direct deoxygenation (DDO) by enhancing C–O bond cleavage. In contrast, SiO_2-supported catalysts exhibited greater Ni dispersion but were more selective toward partially deoxygenated intermediates, such as cyclohexanone and catechol. Among the different temperatures investigated, the HDO at 300 °C maximized fully deoxygenated products, whereas lower and higher temperatures favored partial deoxygenation and hydrogenolysis pathways, respectively.

Keywords Hydrodeoxygenation · Bimetallic catalysts · Bio-oil upgrading · Nb_2O_5 support

1 Introduction

Biomass, particularly lignocellulosic materials such as agricultural residues, wood waste, bagasse, rice husk, and forest debris, offers a viable alternative energy source, especially for challenging sectors such as transportation fuels [1, 2]. This not only provides an alternative to traditional fuels but also empowers farming communities by offering a secondary source of income and reducing the customary burning of agricultural waste [3].

Thermochemical conversion methods, including pyrolysis, hydrothermal liquefaction (HTL), gasification, and combustion, have become economically viable options for converting agricultural waste into energy [4, 5]. Pyrolysis, which occurs at temperatures between 400 and 800 °C in an inert atmosphere, produces solid, liquid, and gaseous fuels. However, the resulting bio-oil is characterized by high oxygen and water contents, as well as high acidity and viscosity, limiting its direct use as a transportation fuel due to its lower heating value compared to conventional fuels [2]. Therefore, oxygen removal and water segregation are essential steps in improving the quality of bio-oil and preparing it for integration into refinery processes [6].

A promising approach to processing bio-oil is catalytic hydrotreating technology, also known as hydrodeoxygenation (HDO). In this method, the bio-oil constituents undergo decarboxylation, decarbonylation, cracking, and

✉ Telis Naiara
naiara.telis@kit.edu

[1] Institute of Catalysis Research and Technology, Karlsruhe Institute of Technology, 76344 Eggenstein-Leopoldshafen, Baden-Wurttemberg, Germany

[2] Faculty of Chemical Engineering, Federal University of Uberlandia, Av. Joao Naves de Avila, Uberlandia, Minas Gerais 38400-902, Brazil

Published online: 03 September 2025

hydrogenation processes, increasing the hydrocarbon content [6]. Bio-oils derived from fast pyrolysis of plant biomass typically contain approximately 40% phenolics and their derivatives, which are building blocks derived from lignin. Among these components, guaiacol has been identified as a representative model compound for evaluating catalysts in HDO due to the presence of two types of C–O bonds (C_{aryl}–OH and C_{aryl}–OCH_3) in its structure [7, 8].

The HDO process can be categorized into two main routes: high-pressure HDO and atmospheric HDO. High-pressure HDO utilizes elevated hydrogen pressure to remove oxygen atoms from oxygenated compounds and hydrogenate aromatic rings. Although atmospheric/low-pressure HDO follows a similar procedure to conventional high-pressure HDO, differences arise in catalyst type, process conditions, reaction mechanism, and the role of hydrogen in the upgrading process [9]. Some studies indicate that HDO using acidic supports, such as Nb_2O_5, offers significant advantages due to the presence of oxophilic sites. These sites promote selective hydrogenation of carbonyl groups or even direct dehydroxylation, leading to valuable deoxygenated products [9, 10].

Makala et al. [11] evaluated the efficiency of deoxygenation in the catalytic HDO of guaiacol using Pd-loaded catalysts on various supports. Their findings revealed a distinct trend in both the reaction rate and deoxygenation product distribution, with Pd/Nb_2O_5 exhibiting the highest efficiency, followed by Pd/TiO_2, Pd/ZrO_2, Pd/CeO_2, and Pd/SiO_2. In this context, NbO_x species play a crucial role, particularly the Nb–O–Nb chains, which demonstrate a strong ability to break the C=O bond [12]. Thus, Nb_2O_5 as a support can enhance the performance of non-noble metals by creating oxygen vacancies that accept lone pair electrons from oxygen in hydroxyl groups. This interaction significantly weakens the C–O bond and accelerates hydrogenolysis, favoring deoxygenation pathways and improving overall catalytic performance.

Recently, Ni-based catalysts have emerged as promising alternatives to noble metals for hydrogenation, given their cost-effectiveness and strong H_2 activation capability. Mortensen et al. [13] demonstrated the hydrogenation ability of Ni catalysts, achieving high yields of cyclohexanol from phenol. However, monometallic Ni catalysts often exhibit low selectivity toward oxygen-free products, such as cyclohexane derivatives. In contrast, Fe, which is more oxophilic than Ni, has been shown to facilitate the hydrogenation of C–O bonds and the hydrogenolysis of C–O bonds in furfural conversion during phenol HDO [14, 15]. Bimetallic Ni–Fe catalysts have been employed in HDO processes [16]. However, these catalysts often display suboptimal selectivity, indiscriminately cleaving oxygen-containing groups such as hydroxyl and methoxyl groups. The previously mentioned advantages of Nb_2O_5 as a support may enhance the performance of the Ni–Fe catalytic system, leading to increased yields of deoxygenated products such as benzene and cyclohexane in the HDO of bio-oils.

This study evaluated the potential of Nb_2O_5 as a support for the Ni–Fe system in the hydrodeoxygenation (HDO) of guaiacol, in comparison to SiO_2 as a support. Given the versatile properties of Nb_2O_5 and its emerging role in catalysis, this work aims to correlate its catalytic performance with the specific properties of Nb_2O_5. The Ni–Fe catalysts and their HDO products were thoroughly characterized to understand how Nb_2O_5 supports influence activity and selectivity.

2 Experimental

2.1 Materials Synthesis

Initially, the support, niobic acid ($Nb_2O_5.nH_2O$, HY-340), provided by CBMM, Brazil, was calcined at 500 °C for 4 h in an air atmosphere, with a heating ramp of 10 °C/min, to obtain the TT-Nb_2O_5 polymorph. Silica (AerosilR OX 50) provided by Evonik, Germany, was similarly calcined under identical conditions to eliminate any adsorbed water.

Subsequently, nickel (Ni) and iron (Fe) precursors, nickel(II) nitrate hexahydrate ($Ni(NO_3)_2{\cdot}6H_2O$, Sigma Aldrich, USA) and iron(III) nitrate nonahydrate ($Fe(NO_3)_3{\cdot}9H_2O$, Sigma Aldrich, USA), respectively, were added in stoichiometric amounts to a flask, along with the calcined support. Wet impregnation was carried out in a rotary evaporator, where the solution was stirred for 8 h.

Subsequently, the water was evaporated at 45 mbar and 35 °C with a rotation speed of 200 rpm until the liquid had completely evaporated. The resulting solid was then dried at 100 °C for at least 12 h and subsequently calcined at 350 °C for 3 h in a static air atmosphere. The catalysts were reduced under a 5% H_2/N_2 atmosphere at 500 °C for 2 h, with a heating ramp of 10 °C/min. After reduction, the catalysts were cooled to room temperature under the same gas flow. Subsequently, passivation was performed by exposing the catalysts to a 5% O_2/N_2 atmosphere for 30 min to stabilize the reduced phases.

2.2 Materials Characterization

For elemental analysis, inductively coupled plasma optical emission spectroscopy (ICP–OES) was conducted using an Agilent 725 spectrometer. Before this, the catalysts were digested via a mixture of HNO_3, HCl, HF, and H_2O_2 in a microwave oven at 240 °C for 45 min, ensuring complete dissolution, particularly of niobium.

The textural properties of the support and calcined catalysts were determined through nitrogen adsorption–desorption measurements via a Micromeritics ASAP 2020 at −196 °C. The samples were pretreated in situ by heating them to 200 °C under vacuum for 12 h to remove surface moisture. The specific surface area was calculated using the BET method.

The crystal structure of the catalysts, both before and after reduction, was analyzed via X-ray diffraction (XRD) using an X'Pert PRO MPD instrument from PANalytical GmbH. Measurements were performed using CuKα radiation within the 2_θ range from 10 to 80°. The average crystal size was estimated via the Scherrer equation, considering instrumental line broadening. Data analysis was conducted using X'Pert High Score Plus software.

For temperature-programmed reduction (TPR), measurements were carried out using an Altamira AMI-300 Series instrument from 3P Instruments GmbH & Co. KG (Altamira distributor for Germany). The samples, in their calcined state, were initially dried by heating to 200 °C under an argon flow, followed by cooling to 30 °C. The reduction was performed by exposing the samples to a 10% H_2/Ar gas mixture while heating from 30 to 850 °C at a rate of 5 °C/min.

The strength and quantity of acid sites in the materials were evaluated via NH_3 temperature–programmed desorption (TPD). A dedicated chemisorption analyzer equipped with a tungsten/rhenium filament thermal conductivity detector (TCD) was used. Before the tests, approximately 100 mg of the sample was reduced in situ under a flow of H_2 (30 mL·min^{-1}) at 500 °C for 2 h. Following this reduction, the samples were dried under helium flow at 450 °C for 130 min and then exposed to a 5% v/v NH_3/He mixture at 100 °C for 60 min.

Excess ammonia was removed by heating to 120 °C under helium flow, and NH_3TPD analysis was performed by heating from ambient temperature to 750 °C at a rate of 3 K/min. The metallic dispersion (D_p) and nickel particle size (d_p) were determined using temperature-programmed hydrogen desorption (H_2-TPD) according to Eqs. 1 and 2 [17].

Before the tests, approximately 100 mg of the sample was reduced in situ under a flow of H_2 (30 mL·min^{-1}, ramp 5 K·min^{-1}) at 500 °C for 1 h. The samples were then cooled to 50°C under an argon flow (ramp 10 K·min^{-1}) and further rinsed for 10 min. The samples were exposed to 33 vol% H_2 in argon for 30 min (10 mL·min^{-1} H_2 + 30 mL·min^{-1} Ar).

Excess H_2 was removed by flushing the sample with pure argon for approximately 90 min. The actual H_2-TPD analysis was performed by heating from ambient temperature to 900 °C at a rate of 10 K·min^{-1}, holding at that temperature for 30 min.

$$D_p\,(\%) = \frac{N_s}{N_t} \times 100 \tag{1}$$

$$d_p = \frac{f}{D_p} \tag{2}$$

where N_s is the number of active sites (the number of chemisorbed molecules multiplied by n, the stoichiometric factor), and N_t is the total number of metal atoms. The factor f depends on the geometry and, for nickel, is 101.2 according to Schmal et al. [17].

The relative number of acidic sites present in the catalysts was determined by NH_3-TPD using an Altamira chemisorption analyzer (AMI-300). The analyzer is equipped with a thermal conductivity detector (rhenium-tungsten) and three mass flow controllers (Hastings Company). The chemisorption equipment was commanded via software ("AMI 300″) from the Altamira software package.

The samples were first reduced under an H_2/Ar stream (20 mL·min^{-1} H_2 + 20 mL·min^{-1} Ar) from 40 to 500 °C with a 5 K·min^{-1} ramp, holding at 500 °C for 1 h. Subsequently, the samples were flushed with helium while cooling to 100 °C (ramp 10 K·min^{-1}). The adsorption of ammonia was performed for 60 min with a flow of 30 mL·min^{-1} of 5% NH_3/He (air–liquid crystal gas mixture). The samples were subsequently flushed for 60 min at 100 °C with 30 mL·min^{-1} pure helium. TPD analysis was carried out from 100 to 700 °C at a heating rate of 5 K·min^{-1} in a 30 mL·min^{-1} pure helium flow.

X-ray photoelectron spectroscopy (XPS) was employed to evaluate the surface composition of the reduced Ni–Fe catalysts. The analysis was performed using a VersaProbe II (ULVAC-PHI Inc.) instrument equipped with an Al K_α monochromatic X-ray source. To preserve anoxic conditions, the prereduced samples were transferred to the instrument's chamber under an argon atmosphere directly from an anoxic glovebox.

2.3 Guaiacol HDO Catalytic Tests

The hydrodeoxygenation (HDO) reaction was conducted in a 200 mL autoclave. For each experiment, 25 g of guaiacol and 1 or 2 g of pre-reduced catalyst were added to the reactor. The reactor used was an autoclave that did not allow in-situ reduction. Instead, the catalysts were reduced externally in a dedicated reduction oven, followed by passivation to stabilize the reduced phases before transfer to the reactor. The autoclave was then sealed, purged with argon to remove any residual air, and pressurized to 5 MPa at room temperature with H_2. The stirrer speed was set to 800 rpm, and the reactor was heated to 300 °C at a controlled heating

rate of 3.33 °C/min. The total reaction time was 3 h, which included a heating period.

According to the literature [18–21], the optimal temperature range for Ni–Fe catalysts in HDO reactions is between 250 and 350 °C. Based on this, catalyst screening was first conducted at 300 °C to identify the best-performing catalyst. Subsequently, a temperature study was performed at 250 °C, 300 °C, and 350 °C with the selected catalyst to evaluate its performance across this temperature range and determine the optimal conditions. After the reaction, the process was quenched by cooling the reactor with compressed air until the internal temperature dropped below 40 °C. Once cooled, a gas sample was extracted for analysis via gas chromatography. The upgraded liquid products were collected, weighed, and analyzed to determine the efficiency of the HDO process. Conversion and selectivity were calculated using the following equations:

$$\text{Selectivity}\ (\%) = \frac{mol of \text{the molecule in the product}}{molodGU\,Aconsumed} \quad (2)$$

$$XGUA\,(\%) = \frac{mol of GU\,Aproduct}{molodGU\,Aconsumed} \quad (3)$$

3 Results

3.1 Characterization of Catalysts

The N_2 physisorption isotherms (75 K) of the supports are shown in Fig. 1, with surface area, pore volume, and average pore diameter values provided in Table 1. According to the classification by the International Union of Pure and Applied Chemistry (IUPAC) [22], all the catalysts, except for SiO_2, exhibited standard type IV isotherms. These type IV isotherms, which are commonly found in heterogeneous catalysts, indicate multilayer adsorption and capillary condensation within mesoporous materials, as described by Schmal et al. [17]. This behavior is typically associated with materials possessing cylindrical pores formed by agglomerates of spheroidal particles with varying sizes and shapes [23].

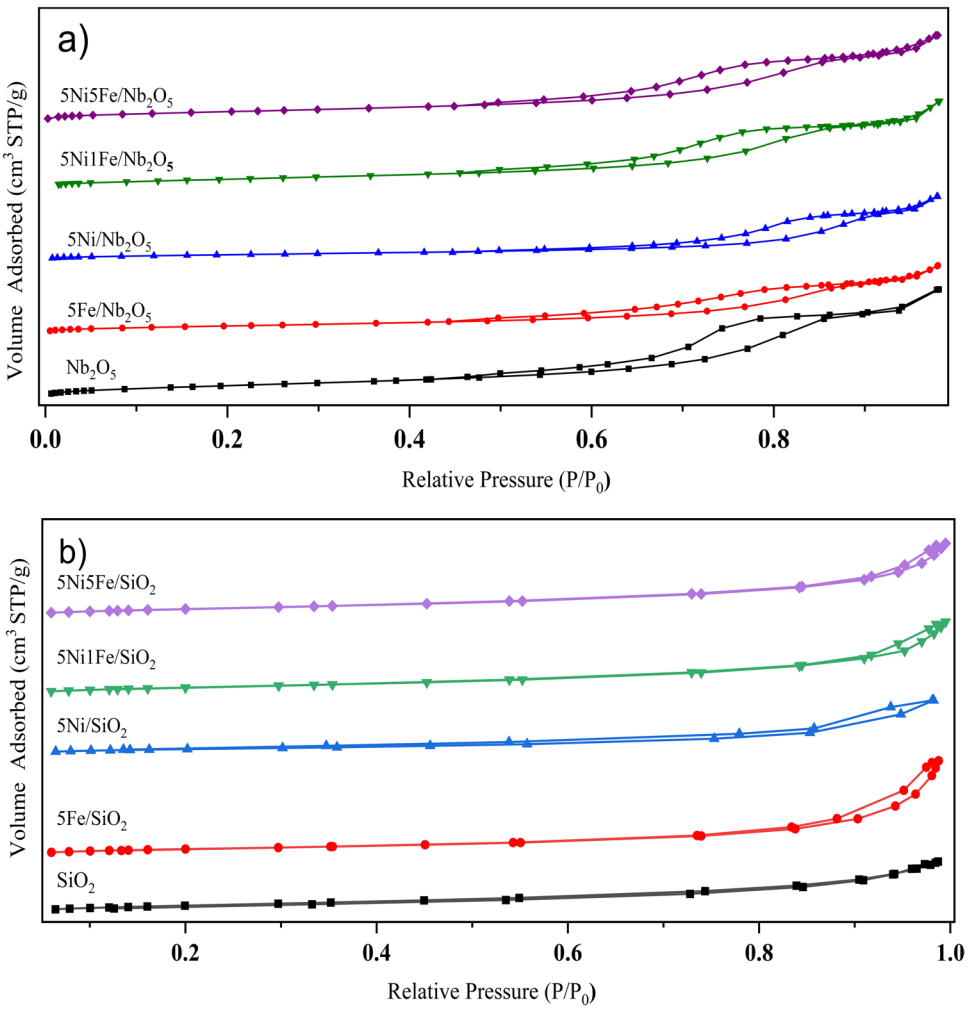

Fig. 1 Textural properties of the (**a**) Nb_2O_5 and (**b**) SiO_2 and supports and the Ni–Fe-supported catalysts

Table 1 Textural properties of the supports used (as determined by N_2 physisorption), average particle size, and metallic dispersion (calculated by H_2-TPD of the reduced catalysts for 2 h at 500 °C)

Samples	Ni (wt.%)	Fe (wt.%)	SBET ($m^2 \cdot g^{-1}$)	V_p ($cm^3 \cdot g^{-1}$)	D_p (%)	Ni Particle Size (nm)
Nb2O5 (500 °C)	0.0	0.0	33.2	0.15	–	–
5Fe/Nb_2O_5	0.0	4.9	32.8	0.10	3.8	–
5Ni/Nb_2O_5	4.9	0.0	24.5	0.09	8.4	11.9
5Ni1Fe/Nb_2O_5	5.0	1.1	42.9	0.12	13.8	18.2
5Ni5Fe/Nb_2O_5	4.9	4.9	41.9	0.12	14.2	15.5
SiO_2 (500 °C)	0.0	0.0	45.2	0.10	–	–
5Fe/SiO_2	0.0	4.7	42.1	0.12	14.4	–
5Ni/SiO_2	4.3	0.0	36.9	0.10	19.3	5.2
5Ni1Fe/SiO_2	4.4	0.9	44.5	0.10	6.1	16.6
5Ni5Fe/SiO_2	4.5	4.9	42.5	0.12	10.1	10.0

The isotherms also feature a narrow hysteresis loop extending to very high relative pressures, close to 0.99, which suggests the presence of large mesopores between the particles. In contrast, the SiO_2 support displayed a type III isotherm, characteristic of weaker gas–solid interactions, as described in the literature [23].

Between the supports Nb_2O_5 and SiO_2, both calcined at 500 °C, niobium oxide (Nb_2O_5) exhibited the lowest specific surface area (33.2 $m^2 \cdot g^{-1}$), consistent with values reported by Zhang et al. and Campos Fraga et al. [10, 22]. In contrast, the calcined SiO_2 support showed a specific surface area of 45.2 $m^2 \cdot g^{-1}$, slightly lower than the precalcination value of 50$m^2 \cdot g^{-1}$ provided by the supplier. Notably, niobic acid (HY-340, $Nb_2O_5.nH_2O$), the precursor for Nb_2O_5, initially possessed a much higher specific surface area of approximately 160 $m^2 \cdot g^{-1}$. However, calcination at 500 °C resulted in a reduction in surface area. This significant decrease is primarily attributed to the collapse of its layered structure and the removal of interlayer water molecules during thermal treatment. Dehydration and structural rearrangement lead to particle agglomeration, pore closure, and densification of the material, thereby diminishing its specific surface area [24, 25]. Furthermore, the incorporation of metallic phases into the supports further decreased the BET surface area due to partial pore blockage by the metallic particles, particularly in the Nb_2O_5-supported catalysts.

The X-ray diffraction (XRD) patterns for the reduced and passivated catalysts are shown in Fig. 2. Silica can exist in either crystalline or amorphous forms, depending on its treatment [26]. In this study, even after the reduction and passivation processes, the support remained amorphous, as indicated by the broad, diffuse band observed at 2θ of approximately 22°, which is characteristic of amorphous silica and consistent with the standard pattern ICSD 176.

With respect to Nb_2O_5, the observed primary structure after calcination was TTNb_2O_5, characterized by a hexagonal lattice, with a prominent peak at $2\theta = 28.6°$, which is consistent with ICSD 1840. The TT-Nb_2O_5 structure, wherein niobium atoms are arranged to create a symmetrical atomic site within an open unit cell, points to a nonstoichiometric composition, specifically $Nb_{16}O_{42}$ [27]. This nonstoichiometry, indicative of an open and adaptable atomic structure, is crucial for the effective impregnation of metal species and their interaction with reactant molecules.

For the calcined samples containing Ni, a distinct NiO peak was observed at $2\theta = 44.3°$ (ICSD 9866). In the diffractogram of 5Ni/SiO_2, the presence of metallic Ni was confirmed, as evidenced by peaks at $2\theta = 44.49°$ and 51.85°, corresponding to the (111) and (200) planes, respectively, and referenced by ICSD 043397. Metallic Ni was also present on 5Ni/Nb_2O_5, indicating that Ni adopted the same phase on both supports.

In the Fe/Nb_2O_5 system, small peaks corresponding to Fe_2O_3 (ICSD 15840) were noted, indicating the presence of low-crystalline Fe oxide species. After reduction, distinct peaks corresponding to Fe_3O_4 (ICSD 26410) and residual Fe_2O_3 were observed. This incomplete reduction was observed in both the Nb_2O_5 and SiO_2-supported catalysts.

Table 2 presents the crystallite sizes of the species observed in the XRD diffractogram calculated via the Scherrer equation. For the Nb_2O_5-supported bimetallic catalysts, specifically 5Ni1Fe/Nb_2O_5 and 5Ni5Fe/Nb_2O_5, we observe crystallite sizes for $FeNb_2O_6$ of 35.5 nm across both catalysts.

The reducibility profiles of the catalysts, as shown in Fig. 3, revealed distinct behaviors for the two different supports. For the 5Fe/Nb_2O_5 catalyst, the initial peak at approximately 277 °C corresponded to the reduction of Fe_2O_3 (Fe^{3+}) to Fe_3O_4 (Fe^{2+}, Fe^{3+}). A subsequent peak at approximately 485 °C indicates the reduction of Fe_3O_4 to metallic Fe (Fe^0) through hydrogen absorption [28].

In contrast, the 5Fe/SiO_2 catalyst exhibited a different reduction pattern (see Fig. 3b), in which Fe_2O_3 had a higher reduction temperature. This suggests that iron is more easily reduced on Nb_2O_5 than on SiO_2 [29]. For comparison, a TPR was also performed with a physical mixture of Fe_2O_3 and Nb_2O_5, and in this case, iron reduction occurred between 330 and 770 °C. As shown in Fig. 3c, two distinct reduction

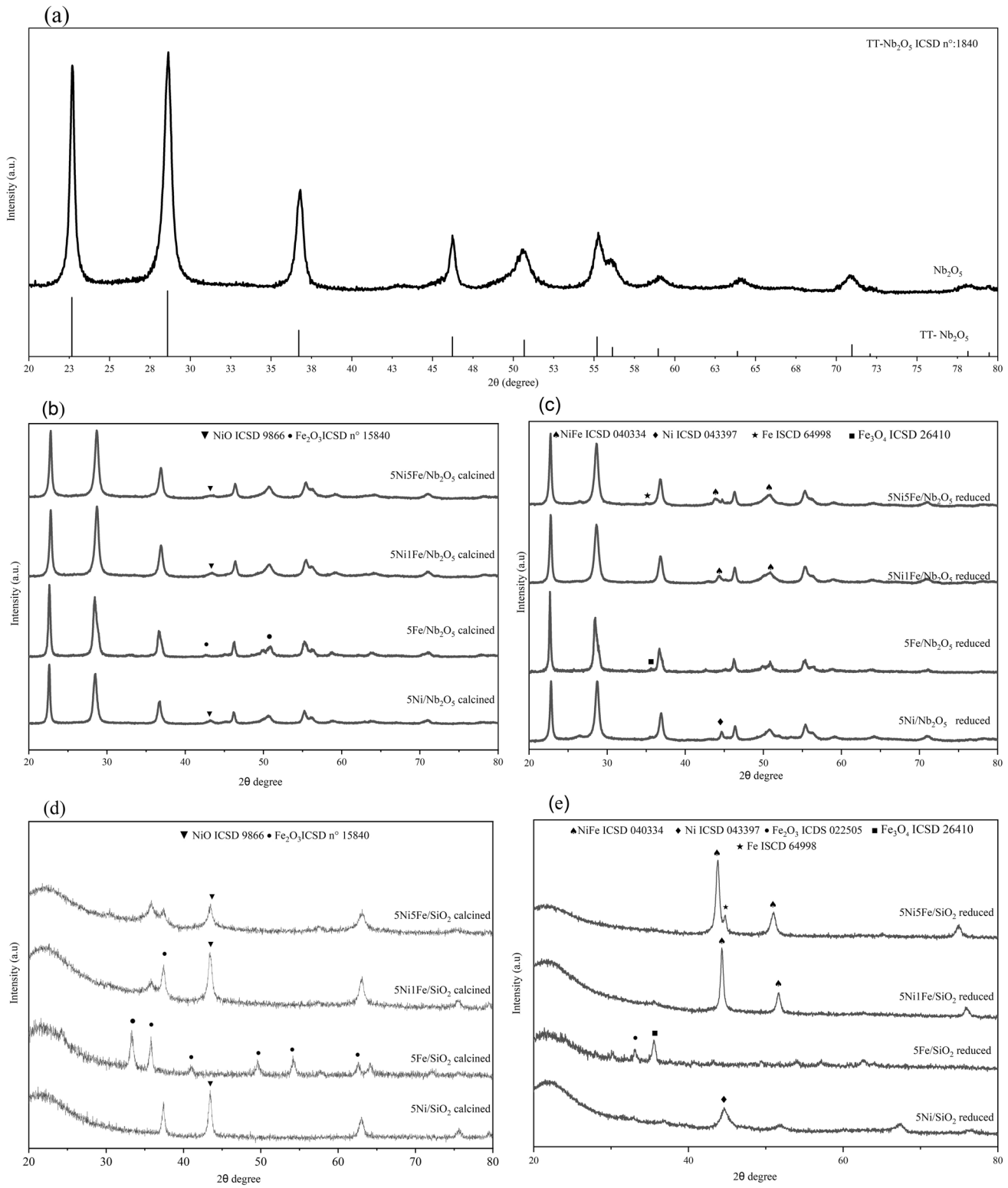

Fig. 2 XRD patterns of the *x*Ni-*y*Fe catalysts with varying metal loadings. The left side represents the calcined catalysts, while the right side shows the reduced catalysts. **a** Nb_2O_5 support, **b** calcined Nb_2O_5-supported catalysts, **c** reduced Nb_2O_5-supported catalysts, **d** calcined SiO_2-supported catalysts, and **e** reduced SiO_2-supported catalysts

Table 2 Crystallite size (τ) (nm) of the catalysts

Sample	NiO	Fe3O4	Fe2O3	$FeNi_3$	Ni	Fe
$5Fe/Nb_2O_5$	–	117	–	–	–	–
$5Ni/Nb_2O_5$	–	–	–	–	116	–
$5Ni1Fe/Nb_2O_5$	–	–	–	21.8	–	–
$5Ni5Fe/Nb_2O_5$	–	–	–	37.8	–	38
$5Fe/SiO_2$	–	49.4	36.3	–	–	–
$5Ni/SiO_2$	77.8	–	–	–	32	–
$5Ni1Fe/SiO_2$	–	–	–	68.1	–	–
$5Ni5Fe/SiO_2$	–	–	–	26.2	–	33

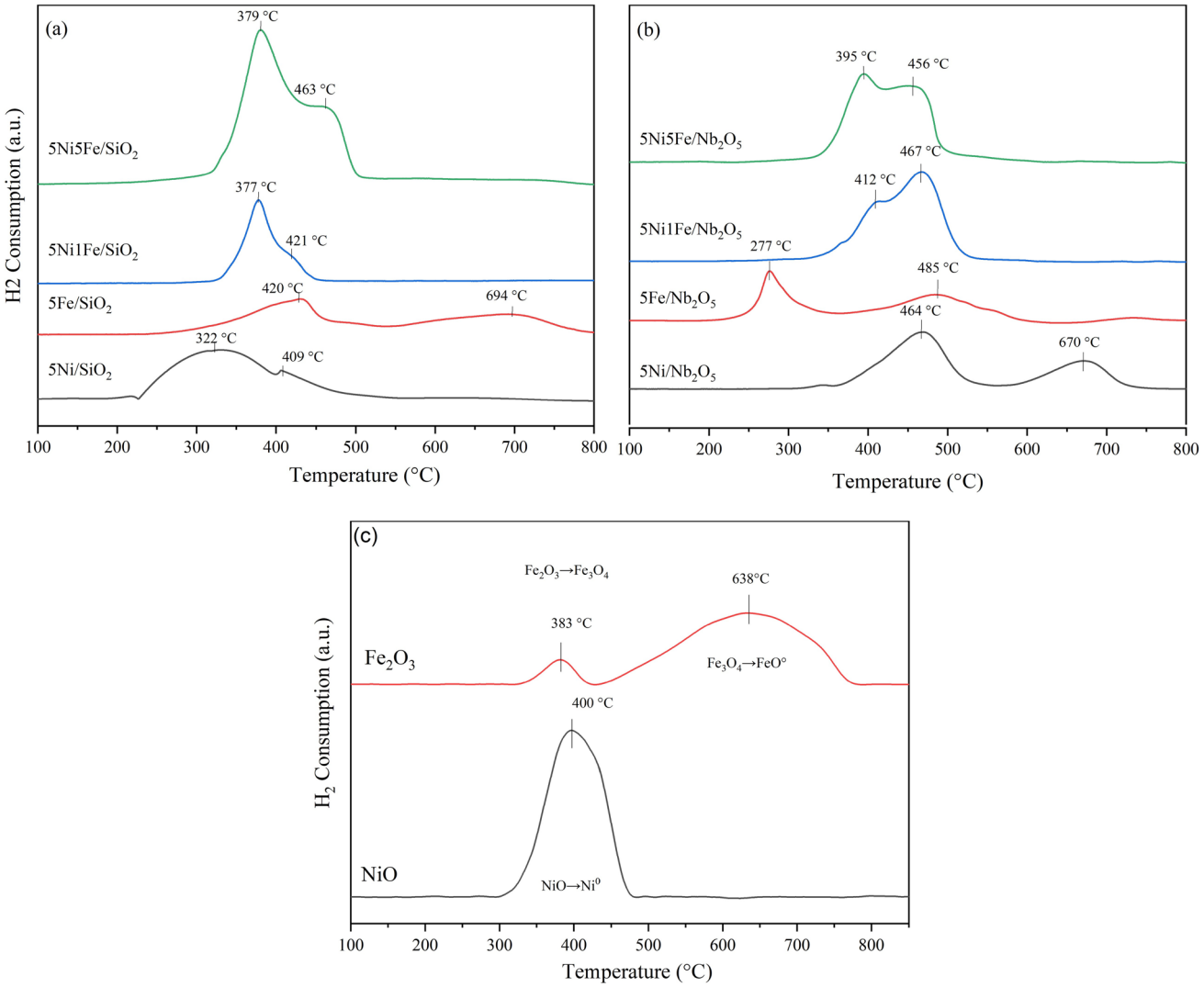

Fig. 3 Temperature-programmed reduction (TPR) profiles of xNi-yFe catalysts with different metal loadings: **a** Nb_2O_5-supported catalysts, **b** SiO_2-supported catalysts, and **c** physical mixtures of metal oxides and Nb_2O_5

peaks were detected: one at 383 °C, corresponding to the reduction of Fe2O3 to Fe_3O_4, and the other at 638 °C, representing the conversion of Fe_3O_4 to metallic Fe (Fe^0). This reduction profile is consistent with findings reported in the literature for iron reduction [30–32].

For the $5Ni/Nb_2O_5$ catalyst, two reduction peaks were observed. The first peak near 464 °C was attributed to the reduction of bulk NiO, whereas the second peak at 670 °C corresponded to the reduction of larger NiO particles and nickel niobate, which are compounds formed during the calcination of the catalysts. Fang et al. [33] reported that

the shoulder peak in the reduction of Ni-based catalysts is associated with the reduction of larger, less dispersed NiO particles. Notably, the interaction between nickel and niobium oxide increased the reduction temperature of nickel, as reported in previous studies (Xu et al., 2022) [34]. In agreement, the shift in the reduction peak observed for the catalyst compared with the TPR of a physical mixture of NiO and Nb_2O_5 points to the presence of a stronger metal–support interaction (SMSI) between the nickel particles and Nb_2O_5 [35]. This shift indicates the presence of Ni^{2+} species that can be easily reduced owing to the presence of oxygen vacancies on the bimetallic catalyst.

Additionally, beyond the interaction between the support and the metals, interactions between Ni and Fe were observed in the 5Ni5Fe/Nb_2O_5 and 5Ni1Fe/Nb_2O_5 catalysts. These bimetallic catalysts demonstrated lower reduction temperatures than their monometallic counterparts and exhibited two distinct reduction peaks. This behavior suggests the formation of a Ni_xFe_y alloy, whose properties are significantly influenced by the Ni/Fe ratio and perform optimally within a specific compositional range, as supported by previous studies [31, 36]. Conversely, when SiO_2 was used as the support, the addition of iron induced a shift toward higher Ni reduction temperatures, reflecting the characteristics of the Fe reduction profile. This trend was evident in both the 5Ni1Fe and 5Ni5Fe/SiO_2 catalysts and can be attributed to the reduction of FeO, facilitated by the Ni–Fe alloy structure. This behavior aligns with the reduction profile of NiO–FeO_x /$MgAlO_x^{-1}$ reported by Huang et al. [19].

The H_2 consumption during catalyst reduction is summarized in Table 3. The monometallic catalysts exhibited relatively consistent H_2 uptake, whereas the differences were more pronounced among the bimetallic catalysts. Specifically, the 5Ni1Fe/Nb_2O_5 catalyst showed higher H_2 uptake (970.28 μmol·g^{-1}) compared to 5Ni1Fe/SiO_2 (719.37 μmol·g^{-1}). In contrast, the H_2 uptake of 5Ni5Fe/SiO_2 (1313.50 μmol·g^{-1}) was comparable to that of 5Ni5Fe/Nb_2O_5 (1076.90 μmol·g^{-1}).

Table 3 Hydrogen uptake and H_2/metal ratios for monometallic and bimetallic catalysts supported on Nb_2O_5 and SiO_2

Catalyst	Uptake (μmol·g^{-1})	H_2/Metal (Theoretical)	H_2/Metal (Real)	Degree of Reduction (%)
Ni/Nb_2O_5	572.49	1.00	0.68	68
Fe/Nb_2O_5	541.11	1.50	0.54	36
5Ni1Fe/Nb_2O_5	970.28	1.33	0.87	65
5Ni5Fe/Nb_2O_5	1076.90	1.33	0.47	35
5Ni/SiO_2	577.48	1.00	0.58	58
5Fe/SiO_2	537.16	1.50	0.46	31
5Ni1Fe/SiO_2	719.37	1.33	0.23	17
5Ni5Fe/SiO_2	1313.50	1.33	0.45	34

H_2 consumption is primarily attributed to the reduction of iron and nickel ions to their metallic states (Fe^0 and Ni^0). The significantly higher H_2 uptake in the 5Ni1Fe/Nb_2O_5 sample compared to 5Ni1Fe/SiO_2 suggests that reducibility is closely linked to catalyst dispersion (Table 1). This trend, where Nb_2O_5-supported catalysts exhibit higher H_2 consumption and improved reducibility compared to SiO_2-supported ones, aligns with the observed catalytic performance, as discussed below.

The support materials (Nb_2O_5 and SiO_2) influenced the hydrogen adsorption properties of the catalysts, as clearly shown by the H_2-TPD profiles of the Ni–Fe catalysts, which revealed distinct desorption peaks. The 5Ni/SiO_2 catalyst exhibited a broad desorption peak (360–650 °C), with the most intense desorption occurring at approximately 470 °C. In contrast, the 5Ni/Nb_2O_5 catalyst showed a broad desorption peak starting at lower temperatures (200–540 °C), with the most intense desorption occurring at approximately 250 °C. This indicates that Nb_2O_5 facilitates better hydrogen desorption on the Ni surface compared to SiO_2, which can enhance the catalytic hydrogenation performance by enabling easier hydrogen release [19].

Both the 5Fe/Nb_2O_5 and 5Fe/SiO_2 catalysts exhibited desorption peaks above approximately 340 °C, indicating strong hydrogen adsorption at the Fe sites [29]. According to the literature [36], desorption temperatures above 300 °C indicate strong surface binding.

As we can see in the Fig. 4 the bimetallic catalyst 5Ni1Fe/Nb_2O_5 exhibited a desorption peak at approximately 381 °C, which can be attributed to the presence of larger Ni particle sizes. In contrast, the 5Ni5Fse/Nb_2O_5 catalyst displayed a broad desorption peak ranging from 220 to 400 °C, with the most intense desorption occurring at approximately 269 °C, likely due to stronger metal–hydrogen bonds facilitated by the presence of Fe molecules [37].

Moreover, the 5Ni1Fe/SiO_2 catalyst exhibited a broader desorption peak at approximately 580 °C, indicating a stronger electronic interaction between Fe and Ni. This characteristic was even more pronounced for the 5Ni5Fe/SiO_2 catalyst.

These results suggest that the SiO_2 support enhanced the interaction between Fe and Ni, resulting in higher temperatures for hydrogen desorption and stronger adsorption sites than those of Nb_2O_5. During desorption, hydrogen atoms on the support migrate back to the metal, where they recombine into hydrogen molecules for release. The high-temperature desorption peaks observed can be explained by hydrogen spillover from the metal to the support, with the spillover rate decreasing as the metal dispersion increases. These findings align with those of Chary et al. [28], who noted that the interaction between the active phase and the support in ruthenium catalysts supported on niobium significantly

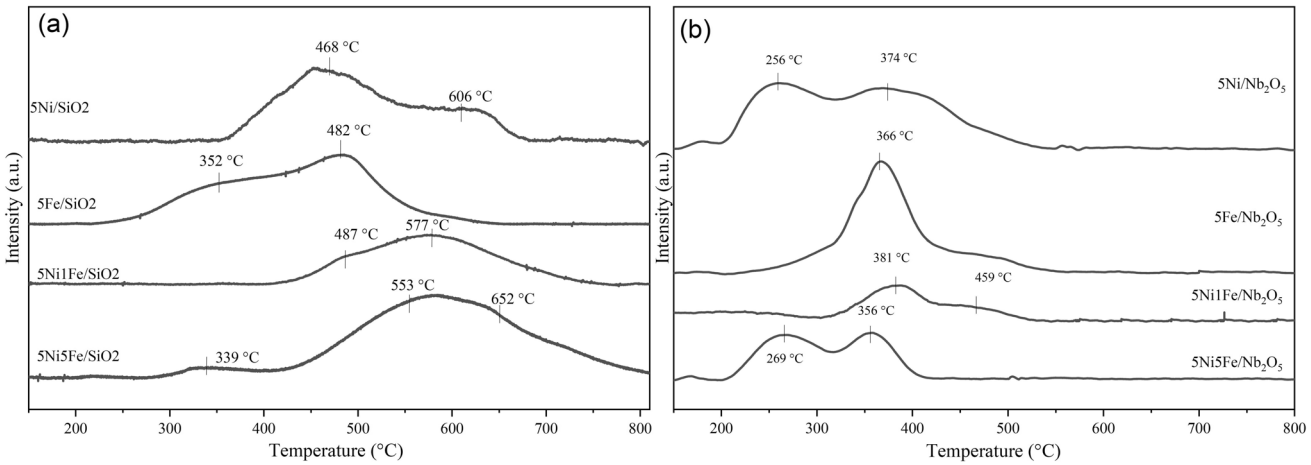

Fig. 4 Hydrogen temperature-programmed desorption (H_2-TPD) profiles of Ni–Fe catalysts: **a** Nb_2O_5-supported catalysts and **b** SiO_2-supported catalysts

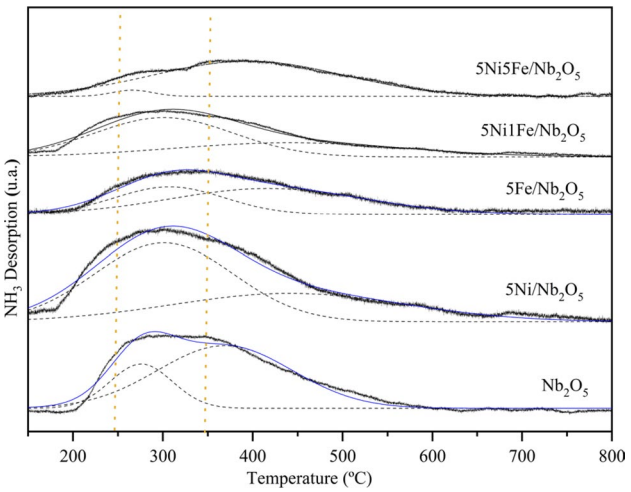

Fig. 5 Ammonia temperature-programmed desorption (NH_3-TPD) profiles of the Nb_2O_5-supported catalysts

influences hydrogen adsorption–desorption behavior, particularly through the hydrogen spillover phenomenon [28, 38].

The density of acid sites in the catalysts was determined via NH_3-TPD, and the desorption profiles are shown in Fig. 5. The Nb_2O_5-supported catalysts exhibited pronounced peaks, reflecting their inherent acidity. In contrast, the SiO_2-supported catalyst (Ni/SiO_2) had almost no NH_3 desorption, suggesting minimal acidity. This observation is corroborated by Campos Fraga (2022) [14]. The profiles, spanning temperatures from 200 to 600 °C, revealed the existence of acid sites varying in strength, categorized as weak (T<249.85 °C), medium (249.85 °C<T>319.85 °C), and strong (T>319.85 °C), on the basis of the temperature range over which ammonia desorption occurs [39]. The presence of multiple peaks within the profiles indicates the presence of acid sites of differing strengths.

Table 4 Total ammonia desorption and the distribution of acid sites (medium and strong) for various catalysts supported on Nb_2O_5 and SiO_2

Sample	Ammonia desorbed ($\mu_{mol/g}$)	Acid sites distribution (%)	
		Medium	Strong
$5Fe/Nb_2O_5$	73	–	100
$5Ni/Nb_2O_5$	80	27	73
$5Ni1Fe/Nb_2O_5$	71	25	75
$5Ni5Fe/Nb_2O_5$	69	30	70
Nb2O5	94	25	75
$5Ni/SiO_2$	7	–	–

The catalysts analyzed presented only medium and strong acid sites, whose densities and distributions are comprehensively detailed in Table 4. Compared with its counterpart $5Ni/Nb_2O_5$, the monometallic $5Fe/Nb_2O_5$ exhibited only strong acid sites but a lower total acidity. The addition of Fe to $5Ni/Nb_2O_5$ led to a reduction in acidity, likely due to the partial occupation or blockage of the acid sites originally present on the Nb_2O_5 support by iron species. This phenomenon is consistent with findings reported by Wang et al. 2022 [40], where increasing Fe doping in a Ce-La oxide system led to significant changes in the NH_3 desorption profile and an increase in overall acidity up to an optimal Fe content. Beyond this point, further Fe addition resulted in structural modifications that altered the acid site distribution and intensity. Similarly, in our case, the further reduction in acidity with increasing Fe content can be attributed to disruption of the support's intrinsic acid sites or dilution of the active Ni species, impairing the synergistic metal–support interaction.

As shown in Fig. 5, these results indicate that Nb_2O_5 has a higher density of acid sites than SiO_2, highlighting the critical role of the support material in determining the catalytic properties of the system.

XPS analysis was performed to examine the surface species and the reduction states of Ni and Fe in the catalysts. All XPS peaks were identified on the basis of an online database (https://srdata.nist.gov/xps/) and published data from the literature. The spectra of the analyzed catalysts are shown in Fig. 6.

The Ni 2p spectra of 5Ni1Fe/Nb_2O_5 and 5Ni5Fe/Nb_2O_5, along with the Fe 2p spectra of 5Ni5Fe/Nb_2O_5, exhibit broad and overlapping peaks, indicating the presence of multiple Ni species with different oxidation states. The binding energy at 855.6 eV was attributed to Ni^{2+}, which is associated with $NiFe_2O_4$ [16, 41] and NiO. Satellite peaks ranging from 857.1 to 859.9 eV further confirmed the presence of Ni^{2+} cations bound to oxygen [21]. Additionally, the peak at approximately 852.1 eV was assigned to metallic Ni^0, indicating the coexistence of oxidized and metallic nickel species. Notably, no Fe 2p signal was observed for 5Ni1Fe/Nb_2O_5 due to its low Fe content. In contrast, the 5Ni5Fe/Nb_2O_5 catalyst presented a Ni/Fe atomic ratio of 0.16, as determined by XPS, which was significantly lower than the ratio of 0.94 obtained via ICP–OES. This suggests Fe segregation on the catalyst surface, likely due to its lower cohesive energy than that of Ni, as reported in previous studies [42, 43]. This segregation supports the hypothesis that Fe tends to segregate on the particle surface because of its lower cohesive energy than that of Ni. The Fe^0 species may interact with Ni^0 to form Ni–Fe alloys within the Ni domains, whereas iron oxides are distributed on the Ni–Fe nanoparticles [40].

The Fe 2p spectra of 5Ni5Fe/Nb_2O_5 revealed a prominent Fe^{3+} peak at 710.4 eV, indicative of abundant oxidized Fe species on the catalyst surface. The peaks at 724.0 eV (Fe $2p_{1/2}$) and 710.4–710.6 eV (Fe $2p_{3/2}$) were attributed to Fe^{3+} species, consistent with the presence of Fe_2O_3 or $NiFe_2O_4$ phases [16, 21, 41]. The absence of XPS signals for the SiO_2-supported catalysts suggests either limited surface accessibility or insufficient surface concentrations of Ni and Fe. These results collectively highlight the influence of metal–support interactions and the surface distribution of active species on catalyst behavior.

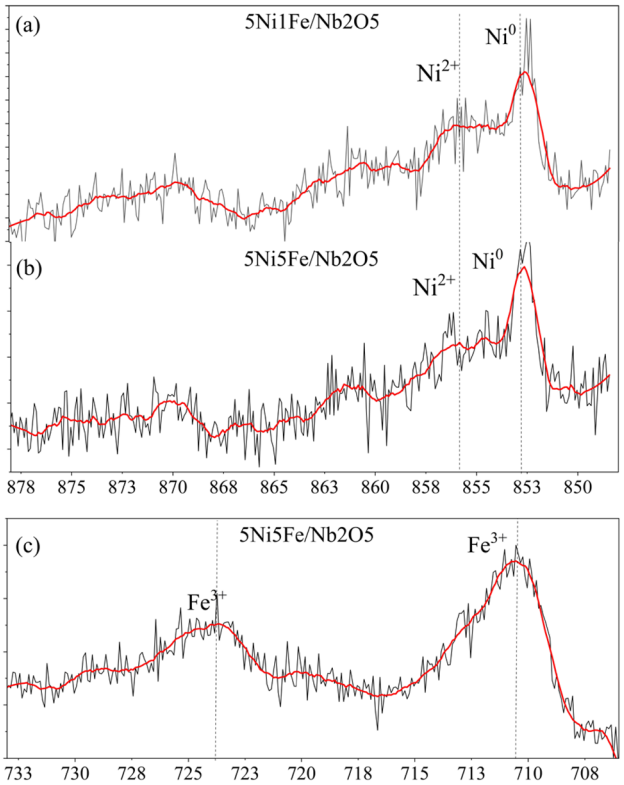

Fig. 6 XPS spectra of Ni 2p for **a** 5Ni1Fe/Nb_2O_5 and **b** 5Ni5Fe/Nb_2O_5 catalysts and **c** XPS spectra of Fe 2p for 5Ni5Fe/Nb_2O_5 catalyst

3.2 Catalytic Performance for HDO of Guaiacol

The hydrodeoxygenation (HDO) of guaiacol at 300 °C demonstrated that bimetallic Ni–Fe catalysts outperformed their monometallic counterparts, particularly in terms of their hydrogenation and deoxygenation activities, as shown in Table 5 and Fig. 7. Among the tested catalysts, 5Ni1Fe/SiO_2 and 5Ni1Fe/Nb_2O_5 exhibited superior hydrogenation of phenolic compounds, with high selectivity toward cyclohexanol. The improved performance can be attributed to the synergistic interaction between Ni and Fe, where Fe contributes to hydrogenolysis activity—crucial for breaking C–O bonds—and Ni facilitates hydrogenation. However, increasing the Fe content in the bimetallic catalysts, as observed for

Table 5 Guaiacol conversion (XGua, %) and normalized product selectivity (%) for various catalysts during hydrodeoxygenation (HDO) at 300 °C

		X Gua (%)	Methanol	Phenol	Catechol	Cyclohexanone	Cyclohexane	Cyclohexanol	Fraction of H2 consumed (%)
Nb_2O_5	5Ni	40	51	34	6	0	0	0	50
	5Fe	40	50	25	11	1	0	0	24
	5Ni1Fe	59	48	3	0	5	10	34	28
	5Ni5Fe	46	50	4	1	5	10	12	49
SiO_2	5Ni	43	48	31	1	13	0	2	49
	5Fe	45	59	8	15	0	0	0	49
	5Ni1Fe	57	41	7	2	15	0	33	82
	5Ni5Fe	41	46	27	3	12	0	9	89

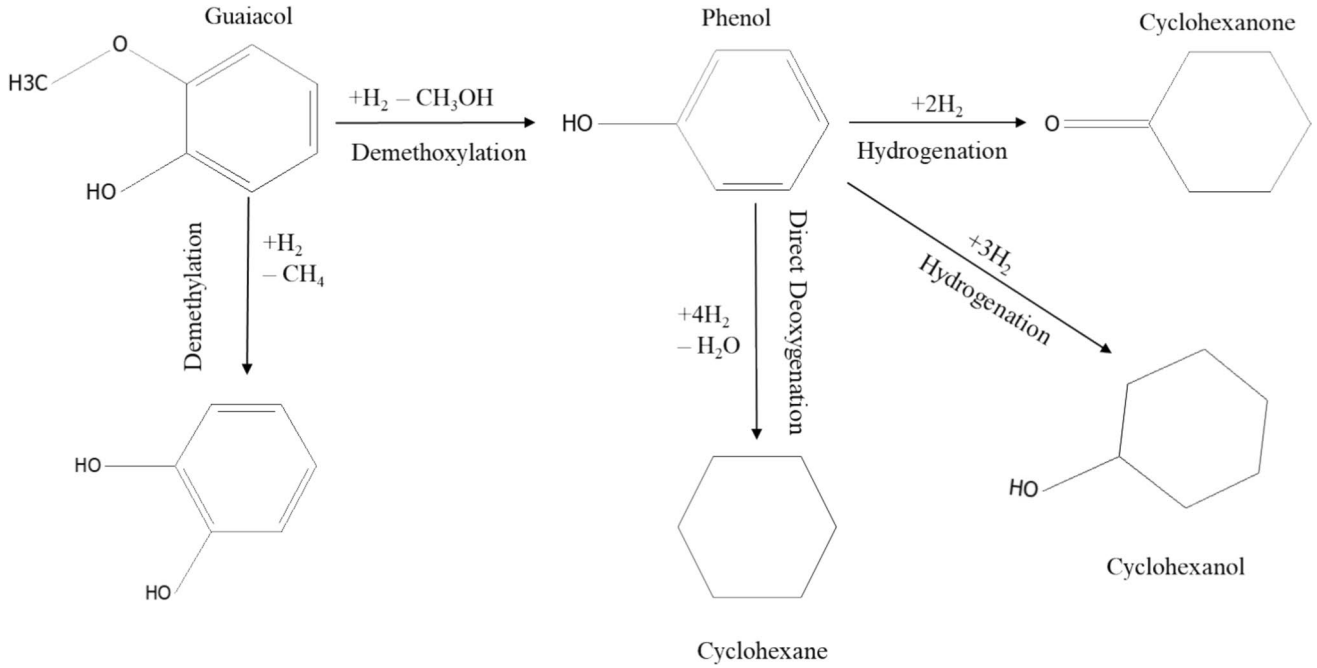

Fig. 7 Proposed reaction pathway for the HDO of guaiacol

5Ni5Fe, resulted in lower guaiacol conversion and reduced selectivity toward cyclohexanol. This selectivity decrease is likely due to excessive Fe content disrupting the Ni–Fe synergy, thereby weakening the hydrogenation capacity of the catalyst, a phenomenon supported in the literature [21, 35, 41]. Due to the non-quantification of carbon deposition (coke) and undetected reaction intermediates in the GC-FID analysis, both the mass and carbon balances closed in the range of approximately 80–85%.

The influence of the support was also critical in determining the catalytic performance. As shown in Table 5, the 5Ni1Fe/Nb_2O_5 catalyst demonstrated the highest deoxygenation activity, indicated by the increased yield of cyclohexane, a fully deoxygenated product. This superior performance is attributed to the unique acidic and oxophilic properties of Nb_2O_5, which favor the direct deoxygenation (DDO) pathway. The oxophilic nature of Nb_2O_5 facilitates cleavage of the C–O bonds, while its acidity promotes dehydration reactions crucial for effective deoxygenation, as confirmed by NH_3-TPD analysis. Moreover, strong metal–support interactions enhance the reduction and dispersion of Ni and Fe, boosting hydrogenation efficiency. Similar observations were reported in the literature, demonstrating that Nb_2O_5-supported catalysts preferentially follow DDO pathways due to the synergistic interaction between the acid sites and metal active phases [39, 43].

In contrast, SiO_2-supported catalysts exhibited higher overall hydrogenation activity but preferentially promoted demethoxylation and hydrogenolysis pathways, resulting in intermediate products such as phenol, catechol, and cyclohexanone. Consequently, the SiO_2-supported catalysts consumed more hydrogen compared to their Nb_2O_5-supported counterparts.

Monometallic Nb_2O_5-supported catalysts, such as 5Ni/Nb_2O_5 and 5Fe/Nb_2O_5, primarily favored partial deoxygenation routes, generating phenol, catechol, and methanol with relatively low hydrogen consumption (50% and 24%, respectively). On the other hand, the bimetallic catalyst 5Ni1Fe/Nb_2O_5 exhibited a clear preference for the direct deoxygenation pathway, leading predominantly to cyclohexanol and cyclohexane. The notably lower hydrogen consumption of 5Ni1Fe/Nb_2O_5 (28%) compared to its SiO_2-supported counterpart (82%) indicates that Nb_2O_5 promotes more efficient hydrogen utilization due to the balanced interaction of acid sites and metal active phases [1, 8].

Additionally, the results align with findings of Yan et al. (2021) [42], which highlighted that bimetallic Ni–Fe catalysts achieve optimal guaiacol conversion and yield at higher Ni–Fe ratios owing to enhanced hydrogenation and hydrogenolysis activity. Fang et al. (2017) [35] also reported that a 5:1 Ni/Fe ratio achieves superior yield for cyclohexane, whereas higher Fe ratios lead to increased phenol yield. In the present study, 5Ni1Fe/Nb_2O_5 exhibited similar trends, further emphasizing the importance of Ni–Fe synergy and the role of Nb_2O_5 in promoting deoxygenation pathways.

3.3 Effect of Metal Sites

Considering monometallic catalysts, the SiO_2-supported ones had smaller metal crystallite sizes than the

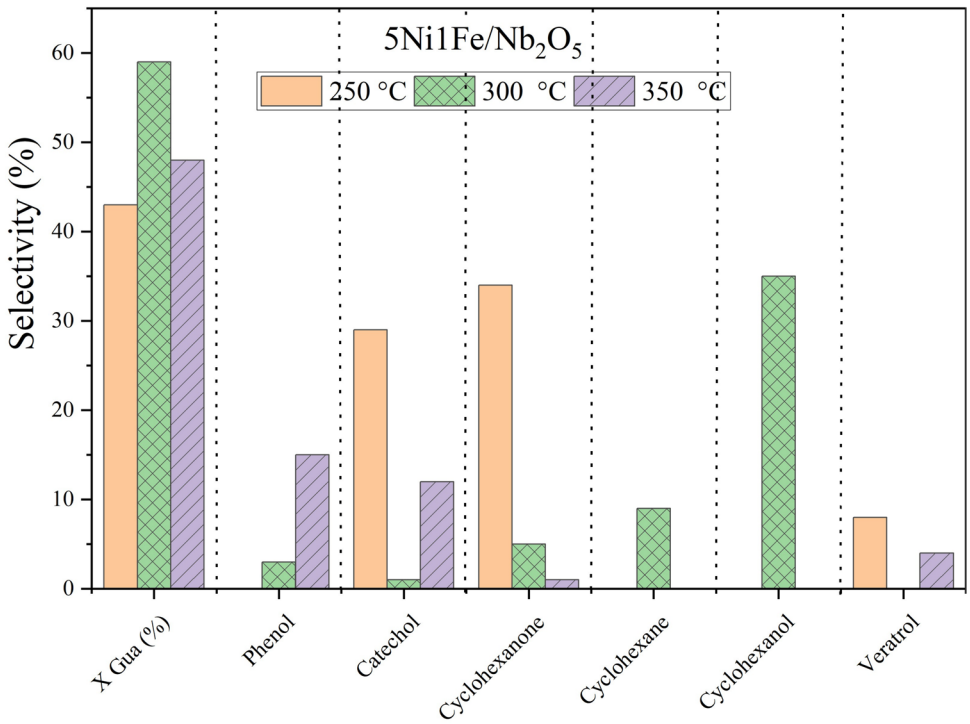

Fig. 8 Effects of reaction temperature (250 °C, 300 °C, and 350 °C) on guaiacol conversion (X_{Gua}, %) and product selectivity during hydrodeoxygenation (HDO) using the 5Ni1Fe/Nb_2O_5 catalyst

Nb_2O_5-supported catalysts and, consequently, better metal dispersion. Between 5Ni/SiO_2 and 5Ni/Nb_2O_5, the SiO_2-supported catalysts presented smaller Ni crystallite sizes (32 nm) and greater dispersion (19.3%). Thus, 5Ni/SiO_2 had slightly higher guaiacol conversion (43%) and significant cyclohexanone production (13%). In agreement, Li et al. (2017) [44] reported that SiO_2-based supports enhance Ni dispersion due to their well-structured mesoporous framework, which prevents metal particle agglomeration and facilitates uniform metal distribution. This observation is supported by the BET surface area measurements in this study, where SiO2 exhibited a higher surface area (45.2 m^2/g) compared to Nb2O5 (33.2 m^2/g), thereby providing more available surface sites for metal dispersion.

On the other hand, the larger Ni particles of 5Ni/Nb_2O_5 (116 nm) resulted in a moderate guaiacol conversion (40%), with methanol (51%) and phenol (34%) as the primary products, suggesting that larger Ni particles limit the availability of active sites and reduce the overall efficiency of the catalyst. Likewise, 5Fe/Nb_2O_5 had Fe crystallites reaching 117 nm, leading to the smallest H_2 consumption (24%) and a strong preference for partial deoxygenation products such as catechol (11%) and phenol (50%).

In contrast, bimetallic 5Ni1Fe/Nb_2O_5 exhibited a smaller metallic crystallite size (NiFe: 21.8 nm) and a better Ni dispersion (13. 8%) than their monometallic counterparts, reflected in higher catalytic performance, with 59% guaiacol conversion and a marked increase in selectivity of cyclohexanol (34%) and cyclohexane (10% This enhancement can be attributed to the synergistic interaction between Ni and Fe, which facilitates hydrogenolysis and hydrogenation, as reported in previous studies [39, 44]. The addition of Fe increased Ni dispersion by inhibiting agglomeration, thus improving the accessibility of active sites, which, in turn, improved hydrogen adsorption and C–O bond cleavage processes.

Finally, the formation of the NiFe alloy, as evidenced by the XRD patterns, further supports the improved catalytic activity of the bimetallic systems. The presence of alloy phases enhances metal–metal interactions, promoting efficient hydrogen activation and deoxygenation pathways. However, catalytic performance is strongly dependent on the Ni:Fe ratio and support properties, as excessive Fe content, despite improving acidity (e.g., NH_3-TPD results), can lead to reduced metal dispersion and diminished catalytic efficiency.

3.4 Influence of Temperature on the Catalytic Performance of 5Ni1Fe/Nb_2O_5

The influence of temperature on product selectivity and guaiacol conversion was investigated using the 5Ni1Fe/Nb_2O_5 catalyst, as shown in Fig. 8. These results, in agreement with observations reported in the literature [42], demonstrate that the reaction temperature plays a crucial role in determining the selectivity of the hydrodeoxygenation (HDO) reaction and the overall reaction pathway [44].

At 250 °C, guaiacol conversion was moderate, and the main products were phenolic intermediates such as phenol and catechol. These findings indicate that at lower temperatures, partial deoxygenation and demethoxylation dominate the reaction mechanism, leading to incomplete HDO. This temperature regime is insufficient to overcome the activation energy required for complete deoxygenation, resulting in the accumulation of oxygenated intermediates.

Increasing the temperature to 300 °C resulted in the highest guaiacol conversion and significant changes in the product distribution. At this temperature, selectivities toward cyclohexane and cyclohexanol were maximized, whereas phenol and catechol were almost entirely absent. This suggests that 300 °C provides the optimal conditions for hydrogenation and deoxygenation pathways, promoting the production of fully deoxygenated products. These results align with those of Wan et al. [45], who reported enhanced hydrogenolysis and reduced hydrogenation with increasing temperature in HDO reactions using Pt/Al_2O_3 at 300 °C, hydrogen availability and adsorption are sufficient to drive the conversion of intermediates into cyclohexane and cyclohexanol.

However, further increasing the reaction temperature to 350 °C caused a decrease in guaiacol conversion and cyclohexane selectivity. This behavior can be attributed to the exothermic nature of hydrogen adsorption on the catalyst surface [11]. At elevated temperatures, the reduced hydrogen coverage likely limits the efficiency of hydrogenation and deoxygenation, resulting in a shift toward hydrogenolysis pathways. This shift is evidenced by the lower selectivity for cycloalkanes and the persistence of phenolic intermediates. Additionally, the selectivity for cyclohexanol decreased significantly, reflecting the unfavorable thermodynamics of hydrogenation at higher temperatures.

The temperature dependence of product selectivity highlights the intricate balance between reaction pathways. At lower temperatures, the reaction favors partial deoxygenation, whereas at intermediate temperatures (300 °C), hydrogenation and deoxygenation dominate. At higher temperatures, the reaction shifts toward hydrogenolysis and possibly the formation of coke precursors. Previous studies [42, 46] have reported that higher temperatures promote the polymerization of oxygen-containing compounds, leading to increased coke formation on the catalyst surface.

These results underscore the importance of temperature optimization in HDO processes. While 300 °C is the optimal temperature to maximize production of fully deoxygenated products such as cyclohexane, higher temperatures can reduce efficiency by limiting hydrogen adsorption and promoting undesired pathways.

4 Conclusion

This study explored the hydrodeoxygenation (HDO) of guaiacol using Ni–Fe bimetallic catalysts supported on Nb_2O_5 and SiO_2, focusing on the synergistic interaction between Ni and Fe and the influence of Nb_2O_5 as a support. The catalysts were thoroughly characterized to correlate their physical and chemical properties with their catalytic activity. Initial screening at 300 °C was performed to identify the most suitable catalyst on the basis of activity and selectivity. The selected catalyst, $5Ni1Fe/Nb_2O_5$, was then used to investigate the impact of the reaction temperature on product selectivity and reaction pathways.

The results of the catalyst screening revealed that the Nb_2O_5-supported catalysts exhibited higher deoxygenation activity than their SiO_2-supported counterparts did. This superior performance was attributed to the acidic properties of TT-Nb_2O_5, which promote the cleavage of the C–O bond and its ability to increase the reduction of Ni and Fe. These factors, combined with the strong synergistic interaction between Ni and Fe, facilitated direct deoxygenation (DDO) pathways, resulting in a significant reduction in oxygenated compounds. In particular, guaiacol conversion to cyclohexane, a fully deoxygenated product, was observed only for the Nb_2O_5-supported Ni–Fe catalysts.

Among the bimetallic catalysts, Fe loading had a critical effect on performance. While the $5Ni1Fe/Nb_2O_5$ catalyst demonstrated superior activity and selectivity toward cyclohexanol and cyclohexane, the higher Fe content in $5Ni5Fe/Nb_2O_5$ disrupted the NiFe synergy, leading to lower guaiacol conversion and selectivity of cyclohexanol.

The temperature-dependent behavior of the selected $5Ni1Fe/Nb_2O_5$ catalyst further highlighted its versatility. At moderate temperatures, products from hydrogenation pathways, such as cyclohexanol and cyclohexane, were favored, reflecting the optimal balance between hydrogenation and deoxygenation. At higher temperatures, the selectivity shifted toward phenol, reflecting the reduced thermodynamic favorability of hydrogenation and a shift toward hydrogenolysis pathways.

In conclusion, this study demonstrates that combining the proven Ni–Fe synergy with the properties of Nb_2O_5 as a support offers a promising approach for efficient HDO processes. The $5Ni1Fe/Nb_2O_5$ catalyst outperformed the other tested catalysts, achieving high guaiacol conversion and selectivity toward fully deoxygenated products. These findings highlight the potential of Nb_2O_5-supported bimetallic catalysts for the sustainable upgrade of bio-oil and provide valuable information on the design of advanced HDO catalysts for renewable energy applications.

Acknowledgements The authors would like to acknowledge CBMM (Companhia Brasileira de Metalurgia e Mineracao) for providing the

raw materials and the Karlsruhe Institute of Technology (KIT) for funding the research. Additionally, the authors acknowledge Birgit Rolli, Yannick Trautlein, and Dieter Schild for their support in analytical measurements.

Author Contributions Not applicable.

Funding Open Access funding enabled and organized by Projekt DEAL. The work was funded by the Ref4Fu project, supported by the Federal Ministry for Digital and Transport Affairs (BMDV) as part of the overall concept for renewable fuels. The funding was coordinated by NOW GmbH and managed by the project management organisations VDI/VDE Innovation + Technik GmbH and the Agency for Renewable Resources (FNR). Open Access funding enabled and organized by Projekt DEAL.

Data Availability The data supporting this study are not publicly available.

Code Availability Not applicable.

Declarations

Conflict of interest The authors declare no conflict of interest.

Ethics Approval and Consent to Participate Not applicable.

Consent for Publication All authors agree with the publication of this manuscript.

References

1. Mishra RK, Kumar V, Kumar P, Mohanty K (2022) Hydrothermal liquefaction of biomass for bio-crude production: A review on feedstocks, chemical compositions, operating parameters, reaction kinetics, techno-economic study, and life cycle assessment. Fuel 316:123377
2. Mishra RK, Mohanty K (2020) Pyrolysis of Manilkara Zapota seeds over ZSM-5 to Produce high-quality bio-oil and chemicals. Fuel 280:118594
3. Magazzino C, Mele M, Schneider N, Shahbaz M (2021) Can biomass energy curtail environmental pollution? A quantum model approach to Germany. J Environ Manage 287:112293
4. Gea S, Hutapea YA, Piliang AFR, Pulungan AN, Rahayu R, Layla J, Tikoalu AD, Wijaya K, Saputri WD (2023) A comprehensive review of experimental parameters in bio-oil upgrading from pyrolysis of biomass to biofuel through catalytic hydrodeoxygenation. Bioenergy Res 16:325–347
5. Mishra RK, Misra M, Mohanty AK (2024) Value-added biocarbon production through slow pyrolysis of mixed bio-oil wastes: studies on their physicochemical characteristics and structure–property–processing co-relation. Biomass Conv Biorefinery 14:7887–7901
6. Zasypalov G, Vutolkina A, Klimovsky V, Abramov E, Vinokurov V, Glotov A (2024) Hydrodeoxygenation of guaiacol over halloysite nanotubes decorated with Ru nanoparticles: effect of alumina acid etching on catalytic behavior and reaction pathways. Appl Catal B 342:123425
7. Mäki-Arvela P, Murzin DY (2017) Hydrodeoxygenation of lignin-derived phenols: From fundamental studies towards industrial applications. Catalysts 7:265
8. Tran QK, Han S, Ly HV, Kim SS, Kim J (2020) Hydrodeoxygenation of a biooil model compound derived from woody biomass using spray-pyrolysis-derived spherical γ-Al_2O_3-SiO_2 catalysts. J Ind Eng Chem 92:243–251
9. Silva NKG, Ferreira RAR, Ribas RM, Monteiro RS, Barrozo MAS, Soares RR (2021) Gas-phase hydrodeoxygenation (hdo) of guaiacol over pt/al_2o_3 catalyst promoted by nb_2o_5. Fuel 287:119509
10. Campos Fraga MM, Vogt J, de Oliveira Campos BL, Schmitt CC, Raffelt K, Dahmen N (2023) Investigation of nb_2o_5 and its polymorphs as catalyst supports for pyrolysis oil upgrading through hydrodeoxygenation. Energy Fuels 37:10474–10492
11. M¨akel¨a E, Gonz´alez Escobedo JL, Neuvonen J, Lahtinen J, Lindblad M, Lassi U, Karinen R, Puurunen RL (2020) Liquid-phase hydrodeoxygenation of 4-propylphenol to propylbenzene: Reducible supports for pt catalysts. ChemCatChem 12:4090–4104
12. Resende KA, Noronha FB, Hori CE (2020) Hydrodeoxygenation of phenol over metal supported niobia catalysts. Renew Energy 149:198–207
13. Mortensen PM, Grunwaldt JD, Jensen PA, Jensen AD (2013) Screening of catalysts for hydrodeoxygenation of phenol as a model compound for bio-oil. ACS Catal 3:1774–1785
14. Campos Fraga MM, de Oliveira Campos BL, Hendrawidjaja H, Carriel Schmitt C, Raffelt K, Dahmen N (2022) Fast pyrolysis oil upgrading via hdo with fe-promoted nb_2o_5-supported pd-based catalysts. Energies (Basel) 15:4762
15. Cheng S, Wei L, Julson J, Muthukumarappan K, Kharel PR (2017) Upgrading pyrolysis bio-oil to hydrocarbon enriched biofuel over bifunctional fe-ni/hzsm5 catalyst in supercritical methanol. Fuel Process Technol 167:117–126
16. Xin H, Yang H, Lei X, Du X, Zhou K, Li D, Hu C (2020) Ni-fe catalysts supported on γ-al_2o_3/hzsm-5 for transformation of palmitic acid into hydrocarbon fuel. Ind Eng Chem Res 59:17373–17386
17. Schmal M, Vargas DC (2016) Spectroscopy in the Infrared Region. Springer, New York
18. Han Q, Rehman MU, Wang J, Rykov A, Gutiérrez OY, Zhao Y, Wang S, Ma X, Lercher JA (2019) The synergistic effect between ni sites and ni-fe alloy sites on hydrodeoxygenation of lignin-derived phenols. Appl Catal B 253:348–358
19. Huang L, Tang F, Liu P, Xiong W, Jia S, Hao F, Lv Y, Luo H (2022) Highly efficient and selective conversion of guaiacol to cyclohexanol over ni-fe/mgalox: understanding the synergistic effect between ni-fe alloy and basic sites. Fuel 327:125115
20. Nie L, De Souza PM, Noronha FB, An W, Sooknoi T, Resasco DE (2014) Selective conversion of m-cresol to toluene over bimetallic ni-fe catalysts. J Mol Catal A 388:47–55
21. Yan P, Kennedy E, Stockenhuber M (2021) Hydrodeoxygenation of guaiacol over BEA supported bimetallic Ni-Fe catalysts with varied impregnation sequence. J Catal 404:1–11
22. Zhang C, Wu J, Hua C, Zhu L, Qiu K, Wang S (2023) Hydrodeoxygenation performance of lignin-derived phenolics to cycloalkanes: Insights into the crystal structures of the nb2o5 support. Energy Fuels 37:14006–14020

23. Leofanti G, Padovan M, Tozzola G, Venturelli B (1998) Surface area and pore texture of catalysts. Catal Today 41:207–219
24. Nowak I, Ziolek M (1999) Niobium compounds: preparation, characterization, and application in heterogeneous catalysis. Chem Rev 99(12):3603–3624
25. Ryu J, Park DS, Hahn BD, Choi JJ, Yoon WH, Kim KY, Yun HS (2008) Photocatalytic TiO_2 thin films by aerosol-deposition: from micron-sized particles to nano-grained thin film at room temperature. Appl Catal B 83(1–2):1–7
26. Nayak PP, Datta AK (2021) Synthesis of sio2-nanoparticles from rice husk ash and its comparison with commercial amorphous silica through material characterization. SILICON 13:1209–1214
27. Gomes GHM, Mohallem NDS (2022) Insights into the tt-nb2o5 crystal structure behavior. Mater Lett 318:132136
28. Gao F, Wang H, Qing M, Yang Y, Li Y (2013) Controlling the phase transformations and performance of iron-based catalysts in the fischer-tropsch synthesis. Chin J Catal 34:1312–1325
29. Jozwiak WK, Kaczmarek E, Maniecki TP, Ignaczak W, Maniukiewicz W (2007) Reduction behavior of iron oxides in hydrogen and carbon monoxide atmospheres. Appl Catal A 326:17–27
30. Insyani R, Kim MK, Choi JW, Yoo CJ, Suh DJ, Lee H, Kim CS, Kim KH, Kim K, Ha JM (2022) Selective hydrodeoxygenation of biomass pyrolysis oil and lignin-derived oxygenates to cyclic alcohols using the bimetallic NiFe core-shell supported on TiO2. Chem Eng J. https://doi.org/10.1016/j.cej.2022.136578
31. Meng F, Zhong P, Li Z, Cui X, Zheng H (2014) Surface structure and catalytic performance of ni-fe catalyst for low-temperature co hydrogenation. J Chem 2014:534842
32. Sirikulbodee P, Phongaksorn M, Sornchamni T, Ratana T, Tungkamani S (2022) Effect of different iron phases of Fe/SiO2 catalyst in CO2 hydrogenation under mild conditions. Catalysts 12:1–19
33. Fang H, Zheng J, Luo X, Du J, Roldan A, Leoni S, Yuan Y (2017) Product tunable behavior of carbon nanotubes-supported ni–fe catalysts for guaiacol hydrodeoxygenation. Appl Catal A 529:20–31
34. Xu J, Zhu P, El Azab IH, Bin Xu B, Guo Z, Elnaggar AY, Mersal GAM, Liu X, Zhi Y, Lin Z et al (2022) An efficient bifunctional ni-nb2o5 nanocatalysts for the hydrodeoxygenation of anisole. Chin J Chem Eng 49:187–197
35. Zhang Z, Xu H, Li H (2022) Insights into the catalytic performance of ni/nb2o5 catalysts for vanillin hydrodeoxygenation in aqueous phase: the role of nb2o5 crystal structures. Fuel 324:124400
36. Tian D, Liu Z, Li D, Shi H, Pan W, Cheng Y (2013) Bimetallic ni-fe totalmethanation catalyst for the production of substitute natural gas under high pressure. Fuel 104:224–229
37. Geng Y, Li H (2022) Hydrogen spillover-enhanced heterogeneously catalyzed hydrodeoxygenation for biomass upgrading. Chemsuschem 15:e202102495
38. Chary KVR, Srikanth CS, Venkat Rao V (2009) Characterization and reactivity of nb2o5 supported ru catalysts. Catal Commun 10:459–463
39. Shu R, Xu Y, Ma L, Zhang Q, Chen P, Wang T (2017) Synergistic effects of highly active Ni and acid site on the hydrodeoxygenation of syringol. Catal Commun 91:1–5
40. Wang Y, Zhao R, Sun JW, Zhang K, Liu ZX, Zhao ZW, Wu WF (2022) Mechanistic study of ce–la–fe/$_\gamma$-al2o3 catalyst for selective catalytic reduction of no with nh3. Int J Hydrogen Energy 47:8261–8274
41. Shi D, Sadier A, Girardon JS, Mamede AS, Ciotonea C, Marinova M, Stievano L, Sougrati MT, La Fontaine C, Paul S et al (2022) Probing the core and surface composition of nanoalloy to rationalize its selectivity: study of nife/sio2 catalysts for liquid-phase hydrogenation. Chem Catal 2:1686–1708
42. Ojagh H, Creaser D, Tamm S, Hu C, Olsson L (2015) Effect of thermal treatment on hydrogen uptake and characteristics of Ni-, Co-, and Mo-containing catalysts. Ind Eng Chem Res 54:11511–11524
43. Zhang Y, Zou X, Liu H, Chen Y, Dong S, Ji M, Chen D, Xu C, Xie H, Zhu C, Chen T (2021) Perspective on Steam Reforming of Toluene Over Mineral Supported Ni-Fe Catalysts: Essential Roles of Different Structures. SSRN Electronic Journal
44. Li X, Chen G, Liu C, Ma W, Yan B, Zhang J (2017) Hydrodeoxygenation of lignin-derived bio-oil using molecular sieves supported metal catalysts: a critical review. Renew Sustain Energy Rev 71:296–308
45. Wan H, Chaudhari RV, Subramaniam B (2012) Catalytic hydroprocessing of pcresol: metal, solvent and mass-transfer effects. Top Catal 55:129–139
46. Shafaghat H, Rezaei PS, Daud WMAW (2016) Catalytic hydrodeoxygenation of simulated phenolic bio-oil to cycloalkanes and aromatic hydrocarbons over bifunctional metal/acid catalysts of ni/hbeta, fe/hbeta and nife/hbeta. J Ind Eng Chem 35:268–276